

CFBDS J111807-064016: A new L/T transition brown dwarf in a binary system [★]

C. Reylé¹, P. Delorme², E. Artigau³, X. Delfosse², L. Albert³, T. Forveille², A. S. Rajpurohit¹, F. Allard⁴, D. Homeier⁴,
and A. C. Robin¹

¹ Institut UTINAM, CNRS UMR 6213, Observatoire des Sciences de l'Univers THETA Franche-Comté-Bourgogne, Université de Franche Comté, Observatoire de Besançon, BP 1615, 25010 Besançon Cedex, France
e-mail: celine@obs-besancon.fr

² UJF-Grenoble 1 / CNRS-INSU, Institut de Planétologie et d'Astrophysique de Grenoble (IPAG) UMR 5274, Grenoble, F-38041, France

³ Département de physique and Observatoire du Mont Mégantic, Université de Montréal, C.P. 6128, Succursale Centre-Ville, Montréal, QC H3C 3J7, Canada

⁴ Centre de Recherche Astrophysique de Lyon, CNRS UMR 5574, Université de Lyon, École Normale Supérieure de Lyon, 46 allée d'Italie, 69364 Lyon Cedex 07, France

Received ...; accepted ...

ABSTRACT

Stellar-substellar binary systems are quite rare, and provide interesting benchmarks. They constrain the complex physics of substellar atmospheres, because several physical parameters of the substellar secondary can be fixed from the much better characterized main sequence primary. We report the discovery of CFBDS J111807-064016, a T2 brown dwarf companion to 2MASS J111806.99-064007.8, a low-mass M4.5-M5 star. The brown-dwarf was identified from the Canada France Brown Dwarf Survey.

At a distance of 50-120 pc, the 7.7'' angular separation corresponds to projected separations of 390-900 AU. The primary displays no H_α emission, placing a lower limit on the age of the system of about 6 Gyr. The kinematics is also consistent with membership in the old thin disc.

We obtained near-infrared spectra, which together with recent atmosphere models allow us determine the effective temperature and gravity of both components. We derived a system metallicity of [Fe/H]=-0.1±0.1 using metallicity sensitive absorption features in our medium-resolution K_s spectrum of the primary. From these parameters and the age constraint, evolutionary models estimate masses of 0.10 to 0.15M_⊙ for the M dwarf, and 0.06 to 0.07M_⊙ for the T dwarf.

This system is a particularly valuable benchmark because the brown dwarf is an early T: the cloud-clearing that occurs at the L/T transition is very sensitive to gravity, metallicity, and detailed dust properties, and produces a large scatter in the colours. This T2 dwarf, with its metallicity measured from the primary and its mass and gravity much better constrained than those of younger early-Ts, will anchor our understanding of the colours of L/T transition brown dwarfs. It is also one of the most massive T dwarfs, just below the hydrogen-burning limit, and all this makes it a prime probe a brown dwarf atmosphere and evolution models.

Key words. CFBDS J111807-064016 – 2MASS J111806.99-064007.8 – Stars: Low mass, brown dwarfs – binaries: general

1. Introduction

Observational degeneracies between the influences of age, metallicity and effective temperature, hinder our understanding of the physics of atmospheres in the brown dwarf and exoplanetary temperature range. This leads to ambiguities in mapping observational measurements to physical parameters (effective

temperature, mass, gravity, metallicity) using theoretical models. Those are also much less reliable than for stellar objects, in part because the physics of their clouds challenges our understanding.

Brown dwarfs-main sequence star binaries uniquely break most of this degeneracy, because several parameters can be obtained from the better understood primary. Such benchmarks systems are rare, however. When the two components are sufficiently separated to be studied separately, simple spectroscopic observations of the bright primary measure the metallicity of the system and constrain its age. This greatly helps interpreting the spectrum of the brown dwarf, by fixing its age and composition. The photometric distance of the primary – and thus the luminosity of both components – is also less uncertain, and follow-up parallax measurements are more easily carried out. Saumon et al. (2006), studying the atmosphere of Gl 570 D, found the first evidence for departures from local chemical equilibrium in the high atmosphere of T dwarfs, due to the kinetics of nitrogen and carbon chemistry in the presence of vertical mixing. Leggett et al. (2008) showed that then current models can only

[★] Based on observations obtained with MegaPrime/MegaCam, a joint project of CFHT and CEA/DAPNIA, at the Canada-France-Hawaii Telescope (CFHT) which is operated by the National Research Council (NRC) of Canada, the Institut National des Sciences de l'Univers of the Centre National de la Recherche Scientifique (CNRS) of France, and the University of Hawaii. This work is based in part on data products produced at TERAPIX and the Canadian Astronomy Data Centre as part of the Canada-France-Hawaii Telescope Legacy Survey, a collaborative project of NRC and CNRS. Based on observations made with the ESO New Technology Telescope at the La Silla Observatory under programme ID 082.C-0506(A) and the ESO Very Large Telescope at Paranal Observatory under programme ID 385.C-0242(A). Based on observations (director discretionary time) made with the Canada-France-Hawaii Telescope at Mauna Kea Observatory.

fit HN Peg B at the minimum admissible age for the HN Peg system and simultaneously require significant vertical atmospheric mixing. Burningham et al. (2009) used the Wolf 940 system to conclude that model-derived temperatures of very late T dwarfs are 10% too warm. Detailed studies of T dwarf companions to main sequence stars therefore constrain our understanding of T dwarfs in general. Moreover, how often such systems occur and the distributions functions of their orbital parameters constrains theories for brown dwarf formation (Reipurth & Clarke 2001; Bate et al. 2003; Stamatellos & Whitworth 2009).

To date twenty resolved T dwarf-main sequence star systems are confirmed (Table 1). These rare systems constrain cool atmosphere physics regardless of the brown dwarf spectral type, but they are most valuable in temperature ranges that models poorly describe. Our understanding of T dwarf atmospheres is most challenged at the L-T transition, where cloud-clearing processes dramatically change the shape of emerging spectrum. While cool atmosphere models perform relatively well in fully dusty atmospheres (late-M to late-L), in fully dust-free atmospheres (early-T), and in the mid-T dwarfs where low temperature condensates appear (Morley et al. 2012), they do not currently describe the more complex physics at the L/T transition very well (e.g. Allard et al. 2001; Helling et al. 2008).

The transition is observationally characterized by the near-infrared colours swinging from very red, in the late-L and early-T dwarfs, to very blue, in the mid-T dwarfs. This change occurs over a narrow effective temperature range, ~ 1100 to 1400 K (Kirkpatrick et al. 2000; Golimowski et al. 2004; Vrba et al. 2004; Dupuy & Liu 2012). The detection of variability in a few of these objects (e.g. Artigau et al. 2009; Radigan et al. 2012) moreover suggests that cloud coverage is spatially inhomogeneous and further complicates the modeling and interpretation.

This transition is currently poorly constrained observationally. Of the 20 resolved (in seeing-limited observations) binaries of T dwarf and main sequence star, only 5 (Gl 337 D, HD 46588 B, HN Peg B, ϵ Ind Ba, and our discovery) have an early-T secondary, the others harboring mid-late T companions.

We report here the discovery of CFBDS J111807-064016 (hereafter CFBDS 1118), an early T dwarf bound to a mid-M dwarf, 2MASS J111806.99-064007.8 (hereafter 2MASS 1118). We found the brown dwarf in the Canada France Brown Dwarf Survey (CFBDS), a wide field survey for cool brown dwarfs which we conducted with the MegaCam camera (Boulade et al. 2003) on the Canada France Hawaii Telescope (CFHT), and subsequently identified the primary from its common proper motion. In Section 2 we describe our identification of the system and its near-infrared photometric and spectroscopic follow-up. Section 3 examines the physical properties of the system. Section 4 discusses the physical properties of the T dwarf and contrasts them with those of HN Peg B, a T2.5 dwarf with very different age and mass. The last Section summarises our conclusions.

2. Observations

We first identified CFBDS 1118 as a brown dwarf candidate from its red $i' - z'$ colour in the CFBDS. The aims of the survey and its detection techniques are fully described in Delorme et al. (2008b). CFBDS 1118 is undetected in i' , with a 5σ $i' > 24.8$ upper limit), while strongly detected at z' detection ($z' = 22.56 \pm 0.05$). The $i' - z' > 2.3$ (5σ) lower limit made CFBDS 1118 a strong brown dwarf candidate.

Fig 1 shows a J -band image of the brown dwarf, which lies $7.7''$ off a much brighter star identified as 2MASS 1118 (in the 2MASS survey, Skrutskie et al. 2006).

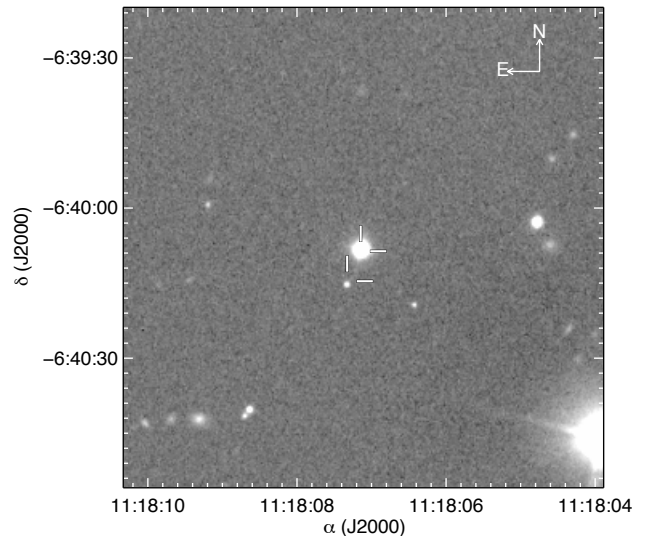


Fig. 1: J -band image obtained with WIRCam at CFHT. The tick marks identify both components, 2MASS 1118 (brighter) and CFBDS 1118 (fainter)

The astrometry, proper motions, and photometry¹ of the components are summarized in Table 2.

Table 2: Positions, proper motions, and photometry of both components. The photometry of the M dwarf is from 2MASS, and the near-infrared magnitudes of the T dwarf are on the 2MASS system. The z' magnitude is on the AB system used by CFHT for MegaCam². The proper motion of the T dwarf is computed between the first and third observation epoch. The proper motions are relative to the mean motion of the stars in the field.

	M dwarf	T dwarf
α	11h18m06.99s	11h18m07.13s
δ	$-06^{\circ}40'07.84''$	$-06^{\circ}40'15.82''$
i'		> 24.86
z'		22.56 ± 0.08
J	13.84 ± 0.03	19.01 ± 0.02
H	13.25 ± 0.02	18.58 ± 0.03
K_s	12.95 ± 0.03	18.30 ± 0.03
μ_α	-201 ± 11 mas/yr	-190 ± 14 mas yr ⁻¹
μ_δ	-49 ± 20 mas/yr	-60 ± 21 mas yr ⁻¹

2.1. Near-infrared photometry

We obtained near-infrared follow-up in the J , H , and K_s -bands in the 2MASS system. Our J -band and H -band imaging respectively consist in twenty 30 seconds, and thirty 20 seconds

¹ Throughout this paper, we use Vega magnitudes for the near-infrared bands and AB magnitudes for the i' and z' optical bands.

² <http://www.cfht.hawaii.edu/Instruments/Imaging/MegaPrime/specsinformation.html>

Table 1: Known binary systems with a main-sequence primary and a T dwarf secondary. The listed physical separations are the projected separations. The last column is the reference of the discovery paper.

Name	Sp. Type		Dist. (pc)	Sep. (AU) (")		Ref.
	Primary	Secondary		(AU)	(")	
Gl 337 CD	K1	L8/T0	20.5	881	43	Wilson et al. (2001); Burgasser et al. (2005)
HD 46588 B	F7	L9	17.9	1420	79.2	Loutrel et al. (2011)
ϵ Ind Ba	K5	T1	3.6	1459	405	Scholz et al. (2003)
CFBDS 1118	M4.5	T2	92	709	7.7	This paper
HN Peg B	G0V	T2.5	18.4	795	43.2	Luhman et al. (2007)
HIP 38939 B	K4	T4.5	18.5	1630	88	Deacon et al. (2012b)
2MASS J03202839-0446358 ^a	M8.5	T5	25	<8.3	<0.33	Burgasser et al. (2008)
SDSS J000649.16-085246.3 B ^a	M8.5	T5	30	—	—	Burgasser et al. (2012)
HD 118865 B	F5	T5	62.4	9200	148	Burningham et al. (2013)
LHS 2803 B	M4.5	T5.5	21	1400	67.6	Deacon et al. (2012a)
ϵ Ind Bb	K5	T6	3.6	1459	405	Scholz et al. (2003)
SCR 1845 B	M8.5	T6	3.8	4.5	1.2	Biller et al. (2006)
HIP 73786 B	K5	T6.5	18.6	1260	68	Scholz (2010)
G 204-39	M3	T6.5	13.6	2685	198	Faherty et al. (2010)
Gl 229 B	M1	T7	5.8	45	7.8	Nakajima et al. (1995)
HIP 63510 C	M0.5	T7	11.7	1200	103	Scholz (2010)
Gl 570 D	K4	T7.5	5.9	1525	258.3	Burgasser et al. (2000)
HD 3651 B	K0	T7.5	11	480	43.5	Mugrauer et al. (2006)
Ross 458 C	M2	T8	11.4	1163	102	Goldman et al. (2010)
LHS 6176 B	M4	T8	18.7	970	52	Burningham et al. (2013)
Wolf 940 B	M4	T8.5	12.5	400	32	Burningham et al. (2009)
GJ 758 B	G9	T9	15.5	29	1.9	Thalmann et al. (2009)

^a unresolved system

long dithered exposures with the SOFI (Moorwood et al. 1998) near-infrared camera on the New Technology Telescope (NTT) at the European Southern Observatory (ESO), La Silla, on March 7, 2009 (Program 082.C-0506(A)). We used a modified version of the jitter utility within the ESO Eclipse package (Devillard 1997) to correct for the flat field, subtract the background and coadd the exposures. We also obtained K_s -band observations of CFBDS 1118 with WIRCam (Puget et al. 2004) at CFHT on March 12, 2012. That sequence consists of 21, 20 s dithered exposures. Table 3 summarizes our imaging observations.

Table 3: Summary of our imaging observations of CFBDS 1118.

Filter	Camera	Exposures	date
z'	CFHT-MegaCam	1x360s	12 April 2007
i'	CFHT-MegaCam	1X500s	5 January 2008
J	NTT-SOFI	20x30s	5 March 2009
H	NTT-SOFI	31x20s	7 March 2009
K_s	CFHT-WIRCam	17x21s	12 March 2012
J	CFHT-WIRCam	5x26s	5 March 2012

We extracted photometry from the resulting images using point spread function fitting within Source Extractor (Bertin & Arnouts 1996) and obtain $J = 19.01 \pm 0.02$, $H = 18.58 \pm 0.03$, and $K_s = 18.30 \pm 0.03$. The resulting $z' - J = 3.55 \pm 0.08$, $J - H = 0.43 \pm 0.03$, and $H - K_s = 0.38 \pm 0.04$ colours confirmed CFBDS 1118 as a brown dwarf at the L/T transition (see e.g. Figs. 1 in Reyl  et al. 2010; Delorme et al. 2012). Besides confirming CFBDS 1118 as a brown dwarf, the photometry will be used to flux-calibrate the spectrum (§2.4).

2.2. Proper motions

The apparent magnitudes ($J = 19.01$ and $J = 13.84$) and colours of the M and T dwarfs places them in a common distance range, 70 to 120 pc from Earth (Sect. 3.1). Comparison of their proper motions further probes whether they form a physical binary.

We first computed the proper motion of the T dwarf from its positions in the z' -band image (observed on April 12, 2007) and in the J -band image (observed on March 07, 2009). That value agreed within 1σ with the proper motion listed in the NOMAD Catalog (Zacharias et al. 2004) for the M dwarf, but was too noisy ($\sigma_{\mu_\alpha} = 64 \text{ mas yr}^{-1}$, $\sigma_{\mu_\delta} = 97 \text{ mas yr}^{-1}$) to strongly exclude a chance alignment.

We therefore obtained a third epoch observation in the J -band with WIRCam at CFHT on March 5, 2012. We did not attempt to reference the astrometry to an absolute frame, as experience shows that this results in larger errorbars, and instead calculated a relative local astrometric solution. This was achieved by cross matching the epochs and using Scamp (Bertin 2006) to reference all astrometric solutions to the first epoch image. Adding the third epoch reduces the error bars on the T dwarf proper motion measurements by a factor of 5, and allows a much stronger test for chance alignment. Table 2 lists those improved measurements.

2.3. Binarity characterization

As Table 2 shows, the proper motions agree to within 1σ . Simulations of the galactic population with the Besan on Galaxy model (Robin et al. 2003) in the direction of CFBDS 1118 shows an only $\sim 3 \times 10^{-5}$ probability that any main sequence star with a proper motion within 3σ of the T dwarf lies by chance in the volume of space delimited by a cone section of $8''$ aperture and 120 pc depth in the direction of CFBDS 1118. Since the CFBDS survey found ~ 70 T dwarfs in CFBDS, the probability that at least one of them would so closely align by chance with an un-

related main-sequence star is just $\sim 2 \times 10^{-3}$. Even one chance alignment within the full survey scale is thus very unlikely, and from thereon we discuss CFBDS 1118 and 2MASS 1118 as a physical binary system.

2.4. Spectroscopic follow-up

We obtained near-infrared spectra of CFBDS 1118 with the XSHOOTER spectrograph (Vernet et al. 2011) on the Very Large Telescope (VLT-UT2) at ESO through Program 385.C-0242(A). The observations were carried out as three 1-hour observing blocks on April 13, 2011, achieving a total exposure time on target of 132 minutes, split into 6 on-the-slit A-B nods of 2×660 s each. The slit width was $1.2''$, and the seeing varied in the range $0.7\text{--}0.9''$. We chose a wide slit, at some cost in increased sky background, because the T dwarf is not visible on the acquisition camera and was set on the slit through a blind offset from the primary. The spectra for individual observing blocks were reduced using the standard ESO XSHOOTER pipeline (Modigliani et al. 2010), which produces a 2-dimensional, curvature-corrected spectrum. We used our own IDL procedures to extract the trace, using Gaussian boxes in the spatial dimension at each wavelength. A similar Gaussian extraction box 5 FWHM off the trace was used to obtain the spectrum of the sky. The resulting 1-dimensional spectrum from each science target observing block was then divided by the spectra of reference stars observed just before or after in order to remove the telluric absorptions. Those were reduced and extracted using the same pipelines. The resulting spectra from the three observing blocks were then median-combined into a final science spectrum. Since that spectrum (with $R = \lambda/\Delta\lambda \approx 3900$) has a low signal to noise ratio, we smoothed the spectra using a weighted average over 100 pixels in the wavelength dimension in the visible arm and over 20 pixels in the near-infrared arm. Our weighting is by the inverse variance of the extracted sky spectrum and therefore uses the full spectral resolution of XSHOOTER to downweight wavelengths affected by telluric emission lines. This improves the signal to noise ratio significantly over simple binning or observations with lower resolution. The final resolution is $R \approx 1100$ and the resulting signal to noise ratio is shown in Figure 2 (upper panel).

The same reduction and extraction procedures were used for the near-infrared and visible arms of XSHOOTER. Given the wide wavelength range covered by XSHOOTER, from 0.6 to $2.5 \mu\text{m}$, seeing variation along the spectral direction can produce wavelength-dependent slit losses. We ensured the flux homogeneity of this wide wavelength spectrum by calibrating it onto our NTT and WIRCcam photometry in the J , H , and K_s -band (Table 2), and onto a near-infrared Y -band magnitude which we estimated from the average colours of a T2 dwarf (Burningham et al. 2013). Following the procedure described in Delorme et al. (2010), we applied small scaling factors to each broadband wavelength ranges to match synthetic photometry derived from the CFBDS 1118 spectrum to its observed photometry. The final spectrum is shown in Figure 2.

We also observed the primary star with XSHOOTER. The M dwarf is detected with a high signal to noise ratio in all XSHOOTER arms (see upper panel in Figure 3) and its spectrum was extracted following the procedures described for the T dwarf. The final spectrum, smoothed using a weighted average over 10 pixels in the wavelength dimension, is shown in Figure 3.

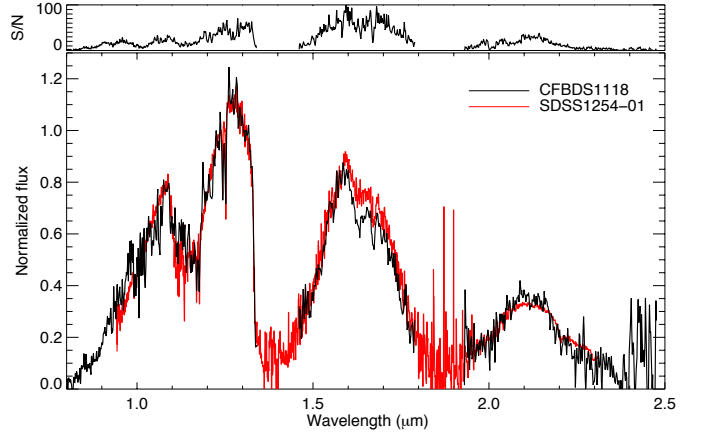


Fig. 2: Black: spectrum of CFBDS 1118 obtained with XSHOOTER at VLT. The regions with strong telluric H_2O absorptions cannot be used and are blanked out. Red: T2 dwarf, SDSS J125453.9-012247 (McLean et al. 2007). A scaling factor is applied to normalize the median flux in the range $1.2\text{--}1.3 \mu\text{m}$ to unity. The upper panel shows the signal to noise ratio.

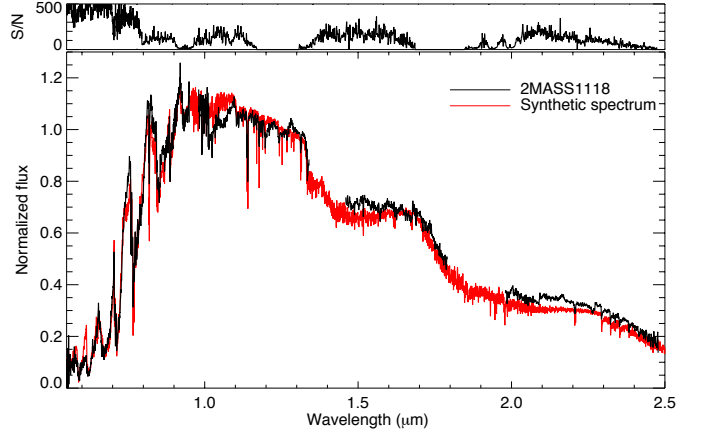


Fig. 3: Spectrum of 2MASS 1118 obtained with XSHOOTER at VLT, in the visible arm ($\lambda < 1 \mu\text{m}$) and the near-infrared arm ($\lambda > 1 \mu\text{m}$). The regions with strong telluric H_2O absorptions cannot be used and are blanked out. The red line shows the synthetic spectrum fitted to derive the astrophysical parameters (see §3). A scaling factor is applied to normalize the median flux in the range $1.2\text{--}1.3 \mu\text{m}$ to unity. The upper panel shows the signal to noise ratio.

3. Physical properties

3.1. Spectral type

We computed spectral indices and derived a spectral type for both component. For the M dwarf, we used the classification scheme defined by Reid et al. (1995) based on TiO and CaH bands strengths. For the T dwarf, we computed the spectroscopic indices defined by Burgasser et al. (2006); Delorme et al. (2008a), which quantify the strength of the key molecular absorption bands, H_2O and CH_4 . Table 4 lists those spectral indices and the corresponding spectral types. This classifies the primary as a M4.5 to M5 dwarf and CFBDS 1118 as a T2 to T3 dwarf. Figure 2 shows the agreement between the spectra of CFBDS 1118 and SDSS J125453.9-012247, a T2 spectral

type standard from the NIRSPEC Brown Dwarf Spectroscopic Survey (McLean et al. 2007).

Table 4: Spectral indices and corresponding spectral type of the two components.

M dwarf		
TiO 5	0.265	M5
CaH 1	0.707	M4.5
CaH 2	0.347	M4.5
CaH 3	0.638	M5
T dwarf		
H ₂ O-J	0.472	T2
CH ₄ -J	0.603	T2
H ₂ O-H	0.482	T2
CH ₄ -H	0.815	T2
CH ₄ -K	0.400	T3

3.2. Photometric distance and separation

In order to compute the photometric distance of 2MASS 1118, we used several M_J versus spectral type relations from the literature, described in Reylé et al. (2006). The M_J absolute magnitude of a M4.5 to M5 dwarf ranges from 8.50 to 9.72, taking into account the uncertainties in the relation, and in particular the discontinuity in the relation at $M_J \approx 8.5$ (or spectral type M3.5/M4.5; Reid & Cruz (2002) discuss this discontinuity in detail). This absolute magnitude range is consistent with $M_J = 9.60$ for Baraffe et al. (1998) evolution models with the stellar parameters estimated in forthcoming sections (3.3, 3.4, and 3.5). This translates to a distance of 67 to 117 pc.

We estimate the distance to the T dwarf with the spectral type vs M_J relation derived by Dupuy & Liu (2012) from brown dwarfs with a measured trigonometric parallax. The absolute magnitude of a field T2 dwarf is $M_J = 14.9 \pm 0.5$, translating to a distance from 51 to 83 pc.

The components are separated by $7.7''$. At the distance of the system, this translates to a projected separation of 393 to 901 AU.

3.3. Kinematics and age

The proper motion translates into a rather high tangential velocity ($77 \pm 30 \text{ km s}^{-1} \text{ yr}^{-1}$), suggesting an old age. The M dwarf spectrum shows no obvious Doppler shift. At the resolution of XSHOOTER, this constrains the radial velocity to a -30 to 30 km s^{-1} interval. From these kinematics, simulations with the Besançon galactic population model (Robin et al. 2003) find 81% probability that the age is above 3 Gyr and 58% probability that it is above 5 Gyr (see Table 5). The older age derived from the kinematics is independently corroborated by the absence of H α emission in the optical spectrum of the primary. According to West et al. (2008), such a low activity level for a mid-M dwarf indicates an age $\gtrsim 6$ Gyr.

3.4. Metallicity

The metallicity of the system can be derived from the K -band spectrum of the primary. As shown by Rojas-Ayala et al. (2010), the metallicity of M dwarfs can be inferred from the strength of their Na I ($2.2 \mu\text{m}$), Ca I ($2.26 \mu\text{m}$) features, together with the

Table 5: Fraction of stars as a function of age simulated with the Besançon Galaxy Model (Robin et al. 2003) in the direction of the system. The distance of simulated stars ranges from 60 to 120 pc, their proper motion μ_α from -230 to -140 mas/yr and μ_δ from -110 to 10 mas/yr , and their radial velocity from -30 to 30 km s^{-1} .

Population	Age	Fraction
Disc	<1Gyr	3%
	1-3Gyr	16%
	3-5Gyr	23%
	5-7Gyr	21%
	7-10Gyr	24%
Thick disc	11Gyr	13%
Halo	14Gyr	0%

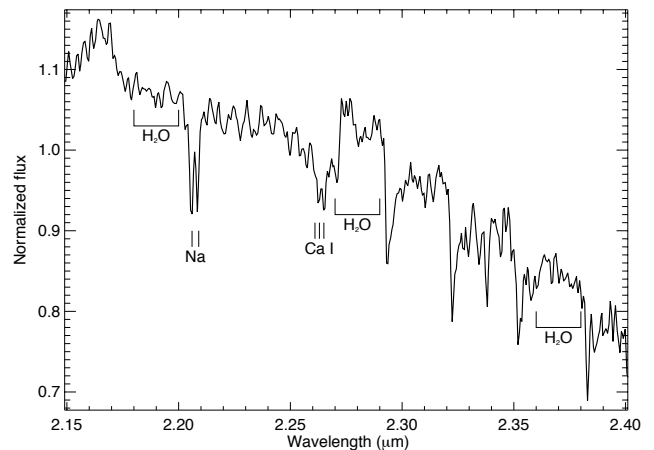


Fig. 4: K -band spectrum of 2MASS 1118 obtained with XSHOOTER at VLT. The features used to compute the metallicity are highlighted.

H₂O-K index defined by Covey et al. (2010). These features are highlighted in Fig 4.

From the Rojas-Ayala et al. (2010); Terrien et al. (2012) relations, the metallicity is $[\text{Fe}/\text{H}] = -0.1 \pm 0.1$ and is consistent with the average metallicity in the solar neighborhood.

3.5. Effective temperature, gravity, and mass

We have compared the most recent version of the BT-Settl stellar atmosphere models (Allard et al. 2012, 2013) with the observed spectra of both components. Those models are computed with the PHOENIX code, and take into account : i) the solar abundances revised by Caffau et al. (2011), ii) the most recent BT2 version of the water vapor line lists by Barber et al. (2008), iii) slightly revised atomic and molecular opacities, iv) a cloud model based on condensation and sedimentation timescales by Rossow (1978), supersaturation computed from pre-tabulated chemical equilibrium, and mixing from 2D radiation hydrodynamic simulations by Freytag et al. (2010). The models are available on-line³ and are fully described in Allard et al. (2012); Rajpurohit et al. (2012); Allard et al. (2013).

The M dwarf spectrum is best fitted by a synthetic spectrum with $T_{\text{eff}} = 3000 \text{ K}$ $\log g = 5.0$ (Fig. 3). The inferred temperature is consistent with the relation between effective temperature scale and spectral sub-type for M dwarfs (see e.g. Fig. 5 in

³ <http://phoenix.ens-lyon.fr/simulator>

Rajpurohit et al. 2013). The Baraffe et al. (1998) evolution models give $\log g = 5.2$ (and a mass of 0.10 to $0.15M_{\odot}$) for an age of 6 Gyr and $T_{\text{eff}} = 3000 \pm 100$ K, which again is reassuringly consistent with the value inferred from the spectrum.

Fig. 5 compares the spectrum of the T dwarf with models of varying effective temperature and gravity. We fixed the metallicity of the models to solar, using our measurement from the near-infrared spectrum of the M dwarf to remove one degree of freedom. A scaling factor is applied to normalize the median flux in the range $1.2\text{--}1.3 \mu\text{m}$ to unity. The best fit, based on visual inspection of Fig. 5, is obtained for $T_{\text{eff}} = 1300$ K and $\log g = 5.0$. However one must be aware that the models still miss some opacity in the H -band. Thus the 1200 K; 4.5 dex and 1400 K; 5.0 dex solutions cannot be excluded.

Table 6 compares these values to those obtained from the (Baraffe et al. 2003) evolution models, when adopting a $T_{\text{eff}} = 1300 \pm 100$ K and for a range of ages. For the age range which we have adopted, the gravity value derived from the model atmosphere fit to the spectrum is inconsistent with that obtained from the evolution models at the fitted effective temperature. This could potentially be due to (i) an erroneous age estimate, or (ii) the known limitations of the cloud model, which is the largest source of uncertainty in brown dwarf atmosphere models. For example, the dust opacity might be poorly estimated due to an incomplete treatment of grain growth mechanisms, which are being addressed in an upcoming revision of the models. The evidence that the system is old, from the low magnetic activity level in the M dwarf and the kinematics of the system, is strong. This leaves (ii) as the most likely explanation.

Table 6: Physical parameters derived from Baraffe et al. (2003) evolution models. The listed temperatures are the closest model grid points to our determination $T_{\text{eff}} = 1300 \pm 100$ K.

Age (Gyr)	Mass (M_{\odot})	T_{eff} (K)	$\log g$	$\log L$ (L_{\odot})	Radius (R_{\odot})
0.5	0.03	1264	4.9	-4.6	0.1
1	0.04	1271	5.1	-4.7	0.09
5	0.06	1120	5.4	-5.1	0.08
5	0.07	1524	5.5	-4.5	0.08
10	0.07	1289	5.5	-4.8	0.08

We therefore adopt the gravity range obtained from the evolution models at old ages, $\log g = 5.4$ at 5 Gyr, and 5.5 at 10 Gyr. This translates into a mass of 0.06 to $0.07 M_{\odot}$ for CFBDS 1118, for ages of respectively 5 and 10 Gyr and a luminosity $\log L/L_{\odot} = -4.80 \pm 0.15$.

4. Discussion

Fig. 6 shows the colour versus spectral type diagram for those L and T dwarfs with $J-K$ photometry measured to better than 0.25 mag and a near-infrared spectral type, as compiled by Dupuy & Liu (2012). The overall trend is a mild reddening of $J-K$ along the L-dwarf sequence, followed by its blueing along the T dwarf sequence. This behavior reflects the evolution of dust grains along the L-dwarf sequence and their settling below the photosphere of T dwarfs, as well as dispersion of the clouds and possibly other unknown mechanism. The diagram shows broad scatter at any given spectral type, most likely arising from differences in metallicity, gravity, and detailed dust clouds properties. Redder colors can result from low gravity, high metallicity, more dust opacity, or a combination of these factors.

The diagram highlights CFBDS 1118, as well as HN Peg B. The latter is a very young $T2.5 \pm 0.5$ dwarf, with an age of just 0.3 ± 0.2 Gyr estimated from its G0 main sequence primary. Its estimated mass is $0.021 \pm 0.009M_{\odot}$, its effective temperature 1130 ± 70 K, and its gravity 4.8 (Luhman et al. 2007; Leggett et al. 2008). The metallicity of the system is -0.01 ± 0.03 (Valenti & Fischer 2005). These two T dwarfs therefore differ widely on age/mass/gravity, and slightly on effective temperature.

Despite their contrasting ages and gravity, CFBDS 1118 and HN Peg B have very similar $J-K$ colours, 0.71 and 0.74. Gravity therefore contributes very little to the $J-K$ scatter of early-T dwarfs, or its effect is compensated by other factors. As the L/T transition marks cloud-clearing, detailed dust properties and cloud coverage may play an important role, as illustrated by the SIMP J1619+0313AB T dwarf binary (Artigau et al. 2011). That system (also shown in Fig. 6) has unexpectedly reversed colours, with a bluer $J-K$ for the earlier-type (T2.5) primary than for the later-type (T4) secondary. The common age and metallicity of the two components leaves contrasting cloud properties, by elimination, as the preferred explanation for the colour reversal (Artigau et al. 2011).

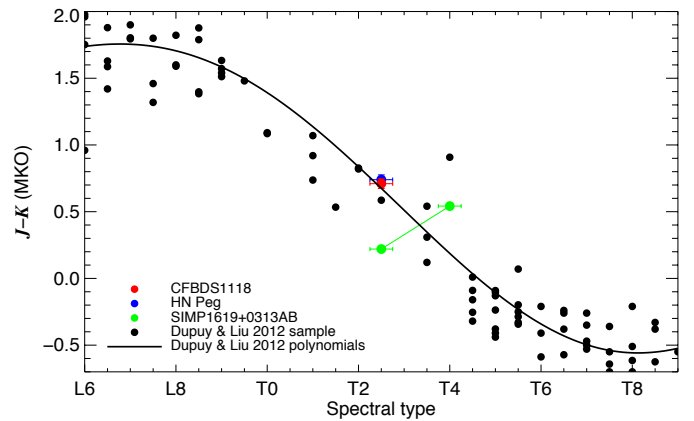


Fig. 6: $J-K$ (MKO) colour versus spectral type for L and T dwarfs. The red and blue markers highlight CFBDS 1118 and HN Peg B, respectively. The green symbols mark the two components of the SIMP 1619+0313AB binary.

Fig. 7 compares the near-infrared spectra of CFBDS 1118 and HN Peg B (from Luhman et al. 2007). The two spectra are extremely similar, with their potassium doublet feature as the main difference. While the young, low-gravity, HN Peg B shows no discernible K I lines, that feature is readily apparent in the CFBDS 1118 spectrum, as expected from its higher gravity (and older age). The increasing strength of K I lines with increasing gravity has been extensively studied in L dwarfs (Allers & Liu 2013), but that trend (mildly) reverses for late-T dwarfs. Those have slightly stronger K I lines at lower gravity, because the CH_4 and H_2O bands which define their pseudo-continuum for the potassium doublet are slightly more sensitive to pressure broadening than is the atomic feature (Allard et al. 2012; Delorme et al. 2012). The two spectra have very similar (normalized) K -band flux, in spite of very contrasting ages and gravities. This contrasts with the late-T dwarfs, where high gravity enhances collision induced absorption by H_2 and, for a fixed effective temperature therefore suppresses the K -band flux with respect to the other bands (e.g. Knapp et al. 2004; Delorme et al. 2012). The $J-K$ colour at the L/T transition is therefore con-

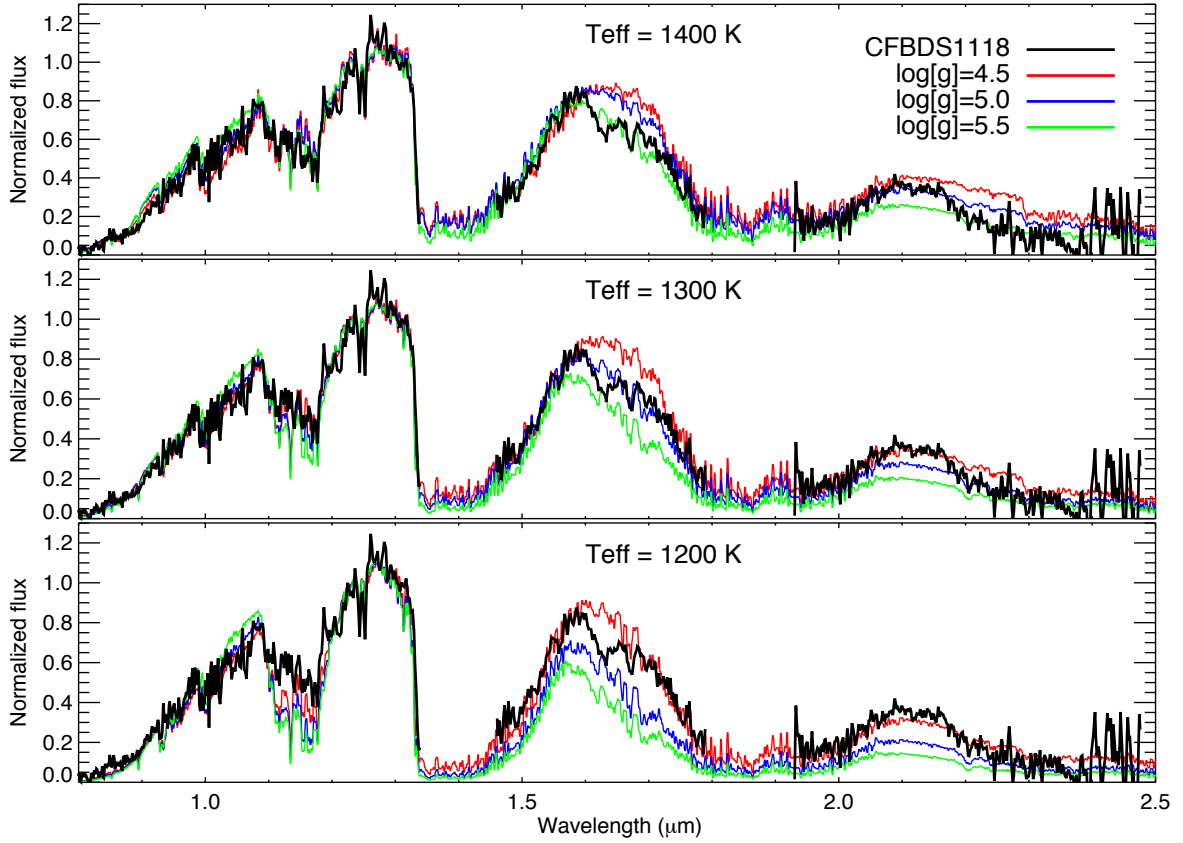


Fig. 5: Comparison of CFBDS 1118 spectrum with BT-Settl models of varying effective temperature and gravity. A scaling factor is applied to normalize the median flux in the range 1.2–1.3 μm to unity. The blue line in the middle panel shows the best fitting model ($T_{\text{eff}} = 1300$ K and $\log g = 5.0$).

trolled by some other parameter, which most likely is dust or cloud-related.

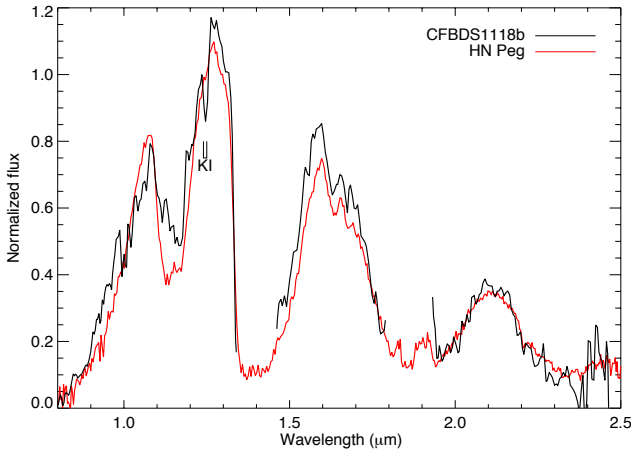


Fig. 7: Spectrum of CFBDS 1118 (black) obtained with XSHOOTER, binned to the resolution of the (Luhman et al. 2007) spectrum of HN Peg B (red) obtained with SpeX at the NASA Infrared Telescope Facility. A scaling factor is applied to normalize the median flux in the range 1.2–1.3 μm to unity. The 1.25–1.26 μm potassium doublet is highlighted.

Fig. 8 shows luminosity against time for different masses for Baraffe et al. (2003) models. The orange dot marks the position of CFBDS 1118. The masses of old (> 5 Gyr) late-L and early-T dwarfs are much better constrained, for a given uncertainty on their luminosity, than those of most sub-stellar objects. At such ages, objects below ~ 60 Jupiter masses have cooled into late-Ts and cooler, while objects above ~ 78 Jupiter masses remain on the bottom of the main sequence and are at most mid-Ls. As a result, old age and an L-T transition spectral type, alone, constrain the mass to $\pm 15\%$. Adding in an even a moderately precise luminosity and an age pinpoints the mass, within the possible systematic errors in the theoretical model grid. As an example, a 20% uncertainty on a $L = 10^{-4.5} L_{\odot}$ luminosity translates into a 3% fractional mass uncertainty at 10 Gyr ($74.9 \pm 2.3 M_{\text{Jup}}$), and into a 13% one at 0.5 Gyr ($36 \pm 5.6 M_{\text{Jup}}$). Given our confidence in its old age, the discrepancies in the physical parameters determined from evolution and atmosphere models of CFBDS 1118 are well established and make an interesting testbed.

5. Summary

Brown dwarfs companions to main sequence stars provide unique benchmarks for studies of cool atmospheres, because the better understood primary star provides the age, distance, and metallicity, of the substellar companion. These systems therefore provide unique tests of cool atmosphere models by vastly reducing the number of degrees of freedom.

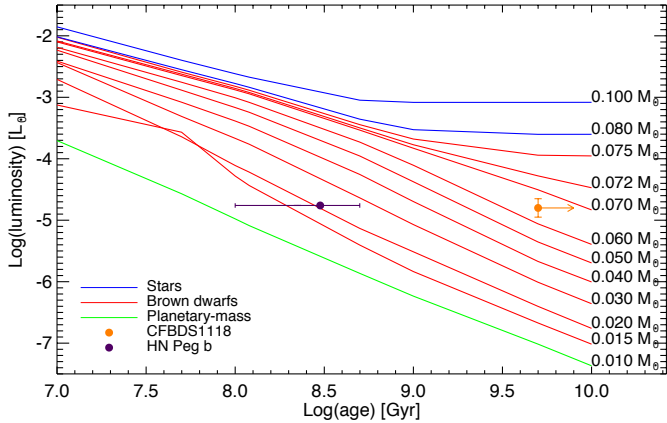


Fig. 8: Luminosity of solar metallicity M dwarfs and substellar objects against time after formation, from Baraffe et al. (2003). The black dot marks HN Peg B and the orange dot shows CFBDS 1118. The luminosity of HN Peg B is $\log L/L_{\odot} = -4.76$, with an error bar of 0.02 (Leggett et al. 2008), smaller than the symbol size.

We identified a $7.7''$ -separation common proper motion M dwarf/T dwarf binary within our CFBD Survey (Delorme et al. 2008b). The red colours of the companion identify it as an early-T dwarf, as confirmed by its spectroscopic follow-up. The high tangential velocity of the system and the low upper limit on the H_{α} feature in the spectrum of the M4.5-M5 primary indicates that the system is old (≥ 5 Gyr). Observations of both components with the wide spectral coverage of XSHOOTER constrain the physical parameters of the system.

The T dwarf, with its metallicity fixed to $[\text{Fe}/\text{H}] = -0.1 \pm 0.1$ from the M dwarf and a well constrained mass estimate, provides a valuable anchor. Thanks to its older age, its properties depend only weakly on its exact age: since older brown dwarfs cool down and contract very slowly (the T_{eff} of a $70 M_{\text{Jup}}$ object, for instance, only drops from 1520 K to 1290 K between 5 and 10 Gyr, and its $\log g$ increase almost insignificantly from 5.47 to 5.50), they are much less affected by the age/mass/luminosity degeneracy that generally hinders field brown studies. The T dwarf also lies close to the boundary between the lowest mass stars (whose luminosity remains constant) and brown dwarfs (with decreasing luminosity). It is one of the most massive brown dwarfs, just below the hydrogen burning limit.

The early-T spectral type of the brown dwarf enhances the value of the system, because the cloud-clearing that occurs at the L/T transition is very sensitive to gravity and metallicity (e.g. Oppenheimer et al. 2013; Allers & Liu 2013). This produces large scatter in the colours, with low gravity objects – such as the late-L type planet 2M1207b (Chauvin et al. 2004) – usually having redder J-K colours. Comparison with HN Peg B, a much younger T2.5 dwarf companion to a main sequence star, however, finds that they have very similar photometric and spectroscopic properties. By contrast, the photometric properties of the two early-T components of SIMP 1619+0313AB system show that they had very different dust dissipation histories in spite of being coevals objects. This suggests that the dust content of the atmosphere, which appears responsible for most of the scatter in L/T transition objects, is not simply controlled by gravity and metallicity: though dust content generally increases with lower

gravity and higher metallicity, several exceptions shows that additional parameters are important.

Acknowledgements. We acknowledge observing support by the CFHT and ESO staffs, and thank the CFHT executive director for granting us discretionary observing time. We acknowledge financial support from "Programme National de Physique Stellaire" (PNPS) of CNRS/INSU, France.

References

- Allard, F., Hauschildt, P. H., Alexander, D. R., Tamanai, A., & Schweitzer, A. 2001, *ApJ*, 556, 357
- Allard, F., Homeier, D., & Freytag, B. 2012, *Royal Society of London Philosophical Transactions Series A*, 370, 2765
- Allard, F., Homeier, D., Freytag, B., et al. 2013, *Memorie della Societa Astronomica Italiana Supplementi*, 24, 128
- Allers, K. N. & Liu, M. C. 2013, *ApJ*, 772, 79
- Artigau, É., Bouchard, S., Doyon, R., & Lafrenière, D. 2009, *ApJ*, 701, 1534
- Artigau, É., Lafrenière, D., Doyon, R., et al. 2011, *ApJ*, 739, 48
- Baraffe, I., Chabrier, G., Allard, F., & Hauschildt, P. H. 1998, *A&A*, 337, 403
- Baraffe, I., Chabrier, G., Barman, T. S., Allard, F., & Hauschildt, P. H. 2003, *A&A*, 402, 701
- Bate, M. R., Bonnell, I. A., & Bromm, V. 2003, *MNRAS*, 339, 577
- Bertin, E. 2006, in *Astronomical Society of the Pacific Conference Series*, Vol. 351, *Astronomical Data Analysis Software and Systems XV*, ed. C. Gabriel, C. Arviset, D. Ponz, & S. Enrique, 112
- Bertin, E. & Arnouts, S. 1996, *A&AS*, 117, 393
- Billier, B. A., Kasper, M., Close, L. M., Brandner, W., & Kellner, S. 2006, *ApJ*, 641, L141
- Boulade, O., Charlot, X., Abbon, P., et al. 2003, in *Presented at the Society of Photo-Optical Instrumentation Engineers (SPIE) Conference*, Vol. 4841, *Instrument Design and Performance for Optical/Infrared Ground-based Telescopes*. Edited by Iye, Masanori; Moorwood, Alan F. M. *Proceedings of the SPIE*, Volume 4841, pp. 72–81 (2003), ed. M. Iye & A. F. M. Moorwood, 72–81
- Burgasser, A. J., Geballe, T. R., Leggett, S. K., Kirkpatrick, J. D., & Golimowski, D. A. 2006, *ApJ*, 637, 1067
- Burgasser, A. J., Kirkpatrick, J. D., Cutri, R. M., et al. 2000, *ApJ*, 531, L57
- Burgasser, A. J., Kirkpatrick, J. D., & Lowrance, P. J. 2005, *AJ*, 129, 2849
- Burgasser, A. J., Liu, M. C., Ireland, M. J., Cruz, K. L., & Dupuy, T. J. 2008, *ApJ*, 681, 579
- Burgasser, A. J., Luk, C., Dhital, S., et al. 2012, *ApJ*, 757, 110
- Burningham, B., Cardoso, C. V., Smith, L., et al. 2013, *MNRAS*, 433, 457
- Burningham, B., Pinfield, D. J., Leggett, S. K., et al. 2009, *MNRAS*, 395, 1237
- Caffau, E., Ludwig, H.-G., Steffen, M., Freytag, B., & Bonifacio, P. 2011, *Sol. Phys.*, 268, 255
- Chauvin, G., Lagrange, A.-M., Dumas, C., et al. 2004, *A&A*, 425, L29
- Deacon, N. R., Liu, M. C., Magnier, E. A., et al. 2012a, *ApJ*, 757, 100
- Deacon, N. R., Liu, M. C., Magnier, E. A., et al. 2012b, *ApJ*, 755, 94
- Delorme, P., Albert, L., Forveille, T., et al. 2010, *A&A*, 518, A39
- Delorme, P., Delfosse, X., Albert, L., et al. 2008a, *A&A*, 482, 961
- Delorme, P., Gagné, J., Malo, L., et al. 2012, *A&A*, 548, A26
- Delorme, P., Willott, C. J., Forveille, T., et al. 2008b, *A&A*, 484, 469
- Devillard, N. 1997, *The Messenger*, 87, 19
- Dupuy, T. J. & Liu, M. C. 2012, *ApJS*, 201, 19
- Faherty, J. K., Burgasser, A. J., West, A. A., et al. 2010, *AJ*, 139, 176
- Freytag, B., Allard, F., Ludwig, H., Homeier, D., & Steffen, M. 2010, *A&A*, 513, A19
- Goldman, B., Marsat, S., Henning, T., Clemens, C., & Greiner, J. 2010, *MNRAS*, 405, 1140
- Golimowski, D. A., Leggett, S. K., Marley, M. S., et al. 2004, *AJ*, 127, 3516
- Helling, C., Ackerman, A., Allard, F., et al. 2008, *MNRAS*, 391, 1854
- Kirkpatrick, J. D., Reid, I. N., Liebert, J., et al. 2000, *AJ*, 120, 447
- Knapp, G. R. et al. 2004, *Astron. J.*, 127, 3553
- Leggett, S. K., Saumon, D., Albert, L., et al. 2008, *ApJ*, 682, 1256
- Loutrel, N. P., Luhman, K. L., Lowrance, P. J., & Bochanski, J. J. 2011, *ApJ*, 739, 81
- Luhman, K. L., Patten, B. M., Marengo, M., et al. 2007, *ApJ*, 654, 570
- McLean, I. S., Prato, L., McGovern, M. R., et al. 2007, *ApJ*, 658, 1217
- Modigliani, A., Goldoni, P., Royer, F., et al. 2010, in *Society of Photo-Optical Instrumentation Engineers (SPIE) Conference Series*, Vol. 7737, *Society of Photo-Optical Instrumentation Engineers (SPIE) Conference Series*
- Moorwood, A., Cuby, J.-G., & Lidman, C. 1998, *The Messenger*, 91, 9
- Morley, C. V., Fortney, J. J., Marley, M. S., et al. 2012, *ApJ*, 756, 172
- Mugrauer, M., Seifahrt, A., Neuhäuser, R., & Mazeh, T. 2006, *MNRAS*, 373, L31
- Nakajima, T., Oppenheimer, B. R., Kulkarni, S. R., et al. 1995, *Nature*, 378, 463

- Oppenheimer, B. R., Baranec, C., Beichman, C., et al. 2013, *ApJ*, 768, 24
- Puget, P., Stadler, E., Doyon, R., et al. 2004, in *Society of Photo-Optical Instrumentation Engineers (SPIE) Conference Series*, Vol. 5492, Society of Photo-Optical Instrumentation Engineers (SPIE) Conference Series, ed. A. F. M. Moorwood & M. Iye, 978–987
- Radigan, J., Jayawardhana, R., Lafrenière, D., et al. 2012, *ApJ*, 750, 105
- Rajpurohit, A. S., Reylé, C., Allard, F., et al. 2013, *A&A*, 556, A15
- Rajpurohit, A. S., Reylé, C., Schultheis, M., et al. 2012, *A&A*, 545, A85
- Reid, I. N. & Cruz, K. L. 2002, *AJ*, 123, 2806
- Reid, I. N., Hawley, S. L., & Gizis, J. E. 1995, *AJ*, 110, 1838
- Reipurth, B. & Clarke, C. 2001, *AJ*, 122, 432
- Reylé, C., Delorme, P., Willott, C. J., et al. 2010, *A&A*, 522, A112
- Reylé, C., Scholz, R.-D., Schultheis, M., Robin, A. C., & Irwin, M. 2006, *MNRAS*, 373, 705
- Robin, A. C., Reylé, C., Derrière, S., & Picaud, S. 2003, *A&A*, 409, 523
- Rojas-Ayala, B., Covey, K. R., Muirhead, P. S., & Lloyd, J. P. 2010, *ApJ*, 720, L113
- Saumon, D., Marley, M. S., Cushing, M. C., et al. 2006, *ApJ*, 647, 552
- Scholz, R.-D. 2010, *A&A*, 515, A92
- Scholz, R.-D., McCaughrean, M. J., Lodieu, N., & Kuhlbrodt, B. 2003, *A&A*, 398, L29
- Skrutskie, M. F., Cutri, R. M., Stiening, R., et al. 2006, *AJ*, 131, 1163
- Stamatellos, D. & Whitworth, A. P. 2009, *MNRAS*, 400, 1563
- Terrien, R. C., Mahadevan, S., Bender, C. F., et al. 2012, *ApJ*, 747, L38
- Thalmann, C., Carson, J., Janson, M., et al. 2009, *ApJ*, 707, L123
- Valenti, J. A. & Fischer, D. A. 2005, *ApJS*, 159, 141
- Vernet, J., Dekker, H., D’Odorico, S., et al. 2011, *A&A*, 536, A105
- Vrba, F. J., Henden, A. A., Luginbuhl, C. B., et al. 2004, *AJ*, 127, 2948
- West, A. A., Hawley, S. L., Bochanski, J. J., et al. 2008, *AJ*, 135, 785
- Wilson, J. C., Kirkpatrick, J. D., Gizis, J. E., et al. 2001, *AJ*, 122, 1989
- Zacharias, N., Monet, D. G., Levine, S. E., et al. 2004, in *Bulletin of the American Astronomical Society*, Vol. 36, American Astronomical Society Meeting Abstracts, 1418